NEON ALGORITHM THEORETICAL BASIS DOCUMENT:
COORDINATE ROTATIONS

PREPARED BY	ORGANIZATION	DATE
Stefan Metzger	FIU	07/01/2013
Jeff Taylor	FIU	11/21/2012

APPROVALS (Name)	ORGANIZATION	APPROVAL DATE
Hanne Buur	CCB DIR SE	05/25/2013
Jeffery Taylor	FIU	05/03/2013

RELEASED BY (Name)	ORGANIZATION	RELEASE DATE
Stephen Craft	SE	07/01/2013

Change Record

REVISION	DATE	ECO #	DESCRIPTION OF CHANGE
A	07/01/2013	ECO-00896	Initial release

TABLE OF CONTENTS

Title: NEON Algorithm Theoretical Basis Document – Coordinate rotations	Author: S. Metzger	Date: 07/01/2013
NEON.DOC.000853		Revision: A

LIST OF TABLES

LIST OF FIGURES

1   DESCRIPTION

NEON shall measure the exchange of momentum, energy and trace gases between the earth's surface and the atmosphere. To accomplish this, NEON will operate an eddy covariance turbulent exchange subsystem (EC-TES, a summary of all notation is provided in Sect. 10), which collectively embodies a suite of sensors.

1.1   Purpose

This document describes the theoretical background and entire algorithmic process for rotating the coordinate basis of (i) the ultrasonic anemometer (SONIC) based three-dimensional (3-D) wind vector measurement in the EC-TES, and (ii) the resulting tensors and vectors of shear stress and scalar fluxes. The present ATBD serves to summarize all corresponding algorithms which will be used during the implementation of AD[01].

1.2   Scope

This ATBD is embedded in a suite of 29 existing and upcoming NEON documents, which collectively describe the acquisition, processing and quality control of data from the EC-TES (AD[01] provides an overview). As such, the scope of this ATBD is to provide all necessary processing steps between immediately preceding and succeeding documents. This ATBD first introduces related documents, acronyms and conventions (Sect. 2). Throughout Sects. 3–7, (i) all reported variables and input variables are identified, (ii) theoretical background is introduced, (iii) explicit conversion algorithms are provided, (iv) error propagation algorithms are provided that enable the calculation of uncertainty budgets for each reported variable, and (v) verification tests are outlined. This document does not provide computational implementation details, except for cases where these stem directly from algorithmic choices explained here.

2 RELATED DOCUMENTS

2.1 Applicable documents

AD[01]	NEON.DOC.000573	Plan for airshed QA/QC development
AD[02]	NEON.DOC.000465	Eddy-covariance turbulent exchange subsystem C^3
AD[03]	NEON.DOC.000651	Atmospheric properties/units ATBD
AD[04]	NEON.DOC.000823	Calculation of variances and covariances ATBD
AD[05]	NEON.DOC.000848	NEON science commissioning and validation plan

2.2 Reference documents

RD[01]	NEON.DOC.000008	NEON Acronym List
RD[02}	NEON.DOC.000243	NEON Glossary of Terms

2.3 Verb convention

"Shall" is used whenever a specification expresses a provision that is binding. The verbs "should" and "may" express non-mandatory provisions. "Will" is used to express a declaration of purpose on the part of the design activity.

3 DESCRIPTION OF VARIABLES

The algorithms in this ATBD provide all necessary processing steps between immediately preceding and succeeding ATBDs in a suite of NEON documents related to the EC-TES (Sect. 1.2, AD[01]). In general, the input variables of this ATBD are generated in preceding EC-TES-related documents, and the reported variables are used in succeeding documents. Which of these variables will be mapped to NEON data products (DP), as well as their corresponding IDs will be defined in succeeding documents, and are not provided in this ATBD.

3.1 Reported variables

Table 1 details the variables reported by the algorithms disclosed in this ATBD. Variables that are to be confirmed and affected algorithms are marked in <mark>yellow</mark>.

Table 1. List of variables that are produced in this ATBD.

Variable	Units
Rotated average wind components ($\bar{u}$, $\bar{v}$, $\bar{w}$)	m s^{-1}
Rotated wind component variances ($\overline{u'u'}$, $\overline{v'v'}$, $\overline{w'w'}$)	m^2 s^{-2}
Rotated covariances ($\overline{u'X'}$, $\overline{v'X'}$, $\overline{w'X'}$)	m s^{-1}·unit[X]
Vertical wind offset ($\widehat{w_0}$)	m s^{-1}
Planar fit rotation angles ($\hat{\alpha}$, $\hat{\beta}$, $\overline{\Psi_{ms}}$)	Decimal degree
Sample sizes N_{PF}, $N(QF_{magn} = 0)$, $N(QF_{PF} = 0)$, $N(QF_{pitch,2} = 0)$, $N(QF_{roll,2} = 0)$	Dimensionless (count)
Quality flags QF_{magn}, QF_{PF}, $QF_{pitch,2}$, $QF_{roll,2}$, QF_{window}	Dimensionless (0 or 1)

3.2   Input variables

Table 2 lists all input variables that are used to produce the output variables reported above. The data sources/DP IDs of these variables are provided when the algorithms in this ATBD are concretely applied during the implementation of AD[01] (e.g. for the determination of the heat fluxes).

Table 2. List of input variables that are used in this ATBD.

Variable	Units
Average SONIC pitch ($\bar{\theta}$)	Decimal degree
Average SONIC roll ($\bar{\phi}$)	Decimal degree
Measured average wind components ($\overline{u_m}$, $\overline{v_m}$, $\overline{w_m}$)	m s^{-1}
Measured wind component variances ($\overline{u'_m u'_m}$, $\overline{v'_m v'_m}$, $\overline{w'_m w'_m}$)	m^2 s^{-2}
Measured covariances ($\overline{u'_m X'}$, $\overline{v'_m X'}$, $\overline{w'_m X'}$)	m s^{-1}·unit[c]
Quality flag for turbulence boom maintenance (QF_{boom})	Dimensionless (0 or 1)

3.3   Product instances

Each NEON site with terrestrial infrastructure will produce an instance of the reported variables in Table 1.

3.4   Temporal resolution and extent

The temporal resolution of all reported variables in Table 1 and input variables in Table 2 is 0.5 h, i.e. the fundamental averaging period of data products derived from the EC-TES. The algorithms disclosed in this ATBD include the fitting of an aerodynamic plane, which by default uses data over a temporal extent of 168 h, i.e., one week.

3.5   Spatial resolution and extent

The input variables used in this ATBD are measured at a single position in space. Consequently both, input variables and reported variables are not spatially resolved. The spatial extent (path length) of all input variables is ≈10 cm (AD[02]). The spatial representativeness of the means, variances and covariances reported in this ATBD is a function of several factors such as measurement height $d_{z,m}$, displacement height $d_{z,d}$, wind speed and -direction, atmospheric stability and surface roughness (AD[03]). From dispersion modeling (e.g., Schmid, 1994, Vesala et al., 2008) it is found that ≈10 $(d_{z,m}-d_{z,d})$ < $d_{x,FP90}$ < 100 $(d_{z,m}-d_{z,d})$, where $d_{x,FP90}$ is the cross-wind integrated upwind extent from within which 90% of an observed value is sourced. The spatial representativeness for each observation of the reported variables will be quantified during the implementation of AD[01].

4   SCIENTIFIC CONTEXT

With the EC-TES, it is our intent to convert measurements of wind speed, scalar concentration *X*, and the resulting eddy flux into estimates of the true surface-air exchange of *X*. For this purpose the measurement is implicitly or explicitly formulated in mathematical statements of the mass balance over a representative patch of surface (AD[01]). The form of these statements depends on the coordinate system in which they are represented, which in turn should be chosen so that the measurements can be used optimally (Lee et al., 2004). In the following we focus on the Cartesian coordinate system, and how to most appropriately align it with the local flow field/topography.

4.1   Theory of measurement/observation

The mass balance of a scalar *X* is the sum of the advective and turbulent fluxes of *X* across each face of a control volume *V*, plus the accumulation of *X* within this volume. If we can measure the fluxes of *X* across each aerial face as well as the rate of change *X* within *V*, we can deduce the transfer across the surface by difference. However, with a point measurement such as the EC-TES we are only able to sample the turbulent flux and the rate of change of *X* at a single point in space. Hence, we are forced to

supply the missing information in other ways, or to make fundamental assumptions (Lee et al., 2004). One of those fundamental assumptions underlying the EC method is divergence-free flow, such as the flow over a plane surface with homogenous vegetation cover. Figure 1 (a) illustrates that in this case mean inflow and outflow (advection) over opposite aerial faces of V offset each other, and satisfying the mass balance requires that advection through the lid of V is insignificant. Hence, while in principle advective and turbulent flows are present, under the zero-divergence assumption only the 3-D turbulent transport is nonzero. This is the quantity measured by the EC-TES. Due to larger vertical gradients, the 3-D turbulent exchange is generally dominated by transport perpendicular to the mean flow (e.g., Finnigan, 1999). This justifies reducing the transport problem to the turbulent flux along the vertical coordinate (1-D).

However, above more complex terrain, divergence of the mean flow can be significant. In Figure 1 (b) streamwise flow divergence is depicted as differing surface areas of the downstream and the upstream aerial face of V. In this example, the surface areas of the lateral faces of V are identical, i.e. the net effect of streamwise flow divergence is not compensated by lateral flow divergence. In such a case, satisfying the mass balance for a given period of time would require advection through the lid of V, i.e. transport through a non-zero mean wind perpendicular to the mean flow. It is evident from the mass balance approach that the horizontal flux budget cannot be quantified using a single point measurement alone. Adequate measurement strategies are subject of ongoing research (e.g., Aubinet et al., 2012). Yet, compared to the aerial faces of V, the earth's surface provides a quasi non-permeable boundary condition with regard to mass transport. Hence, a single point measurement can nonetheless provide valuable information on the turbulent and advective parts of the exchange perpendicular to the surface.

(a)

(b)
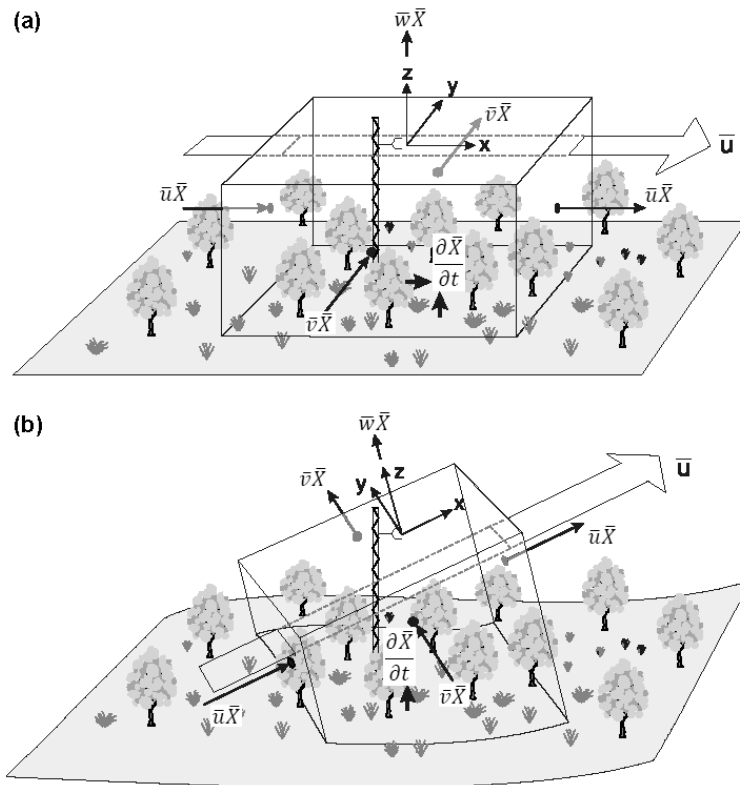
Figure 1. Modified after Finnigan (2004): Control volumes with Cartesian coordinates *x*, *y*, *z*, corresponding wind components *u*, *v*, *w*, scalar concentration *X* and overbars denoting mean quantities. (a) Homogeneous terrain. The coordinate axes are aligned with the mean streamline, which is parallel to the surface as is the lid of the control volume. (b) Complex topography. The *y-z* coordinate plane is defined by an ensemble of mean streamlines and the lid of the control volume is not parallel to the average surface.

This information will be used during quality assessment and quality control of the measurements (Sect. 4.3, AD[01]) Regardless of terrain complexity, the mean streamlines flowing over the landscape will align with the terrain surface, and can thus provide an appropriate coordinate reference (e.g., Baldocchi et al., 2000). To minimize cross-contamination between flows along the *x*, *y*, *z* coordinates and to enable the optimal extraction of information, the EC-TES measurement should be aligned with the mean streamlines. However, in particular, over complex terrain the orientation of the streamlines relative to the SONIC can vary with (i) wind direction, (ii) seasonal cycles and associated state of vegetation foliage, and (iii) sensor alignment. Hence, coordinate rotation is a necessary step before the observed fluxes can be meaningfully interpreted. This procedure is also called tilt correction (e.g., Foken, 2008).

Here, we identify three general methods to align the vector basis of the right-hand Cartesian coordinate frame of the SONIC with the average streamlines;

4.1.1 Double rotation method (Kaimal and Finnigan, 1994, McMillen, 1988, Tanner and Thurtell, 1969);

Tanner and Thurtell (1969) define the natural wind vector basis such that, for each averaging period individually, the *x-y* plane is rotated parallel to the observed mean flow. Transformation from the instrument coordinate to the natural wind coordinate is accomplished by a two-step rotation, first around the *x*-axis (azimuth), and subsequently around the *y*-axis (pitch). In this way the measured lateral ($\overline{v_\mathrm{m}}$) and vertical ($\overline{w_\mathrm{m}}$) wind components during each averaging period are forced to zero. In an idealized homogeneous flow, this serves the function of leveling the anemometer to the surface. However, over more complex terrain the pitch rotation angle can vary systematically with azimuth (Figure 2, top left panel). Substantial scatter/over-rotation in the pitch angle can result from compensating the full magnitude of $\overline{w_\mathrm{m}}$, which may also include transient advective flows ($\overline{w} \neq 0$) in addition to the long-term terrain-forced flow ($\widehat{w}$).

4.1.2 Planar fit (PF) method (Kondo and Sate, 1982, Lee et al., 2004, Mahrt et al., 1996, Wilczak et al., 2001);

If the azimuthal function of the pitch angle approximates a sinusoidal function, the combination of instrument alignment and terrain tilt corresponds to a tilted plane. This behavior results because $\overline{w_\mathrm{m}}$ is positive when air flows up the hill, it is negative when it flows down the slope, and it is zero when the wind is aligned across the slope (Baldocchi et al., 2000, Rannik, 1998). With the assumption that the surface is uniformly tilted, such plane can be regressed between an ensemble of observations of the mean vertical wind and the mean horizontal wind components (e.g., Wilczak et al., 2001). In contrast to the double rotation method, the regressed plane offers a consistent frame of reference for the period of time covered by the ensemble (Figure 2, top right panel). Consequently, it also provides a more representative estimate of the long-term terrain-forced flow $\widehat{w}$. In addition, (i) the regression residuals

$\overline{w} \neq 0$ are indicative of transient advective flows, (ii) the uncertainty in the regression coefficients yields a way to quantify uncertainty in the coordinate rotation, and (iii) systematic changes in instrument tilt/terrain properties over time are indicated by corresponding changes in the regression coefficients. To enable these interpretations, the ensemble of observations must be chosen to be representative of the longer-term 3-D flow at a measurement location. As a result several restrictions apply to the selection of suitable observations, which are specified in Sect. 5.3.

4.1.3 Surface fit method (Baldocchi et al., 2000, Finnigan, 1999, Lee, 1998, Paw U et al., 2000).

If the azimuthal function of the pitch angle is not sinusoidal, the terrain (actually, the mean 3-D flow pattern) does not exhibit a uniform tilt (Figure 2, bottom right panel). For example, over an area with several small hills and valleys one arrives at some relationship between the vertical transform angle and the azimuthal transform angle (e.g., Lee, 1998). Such relationship can be fitted by a polynomial, or for more complex terrain a non-linear surface regression can be used (Paw U et al., 2000).
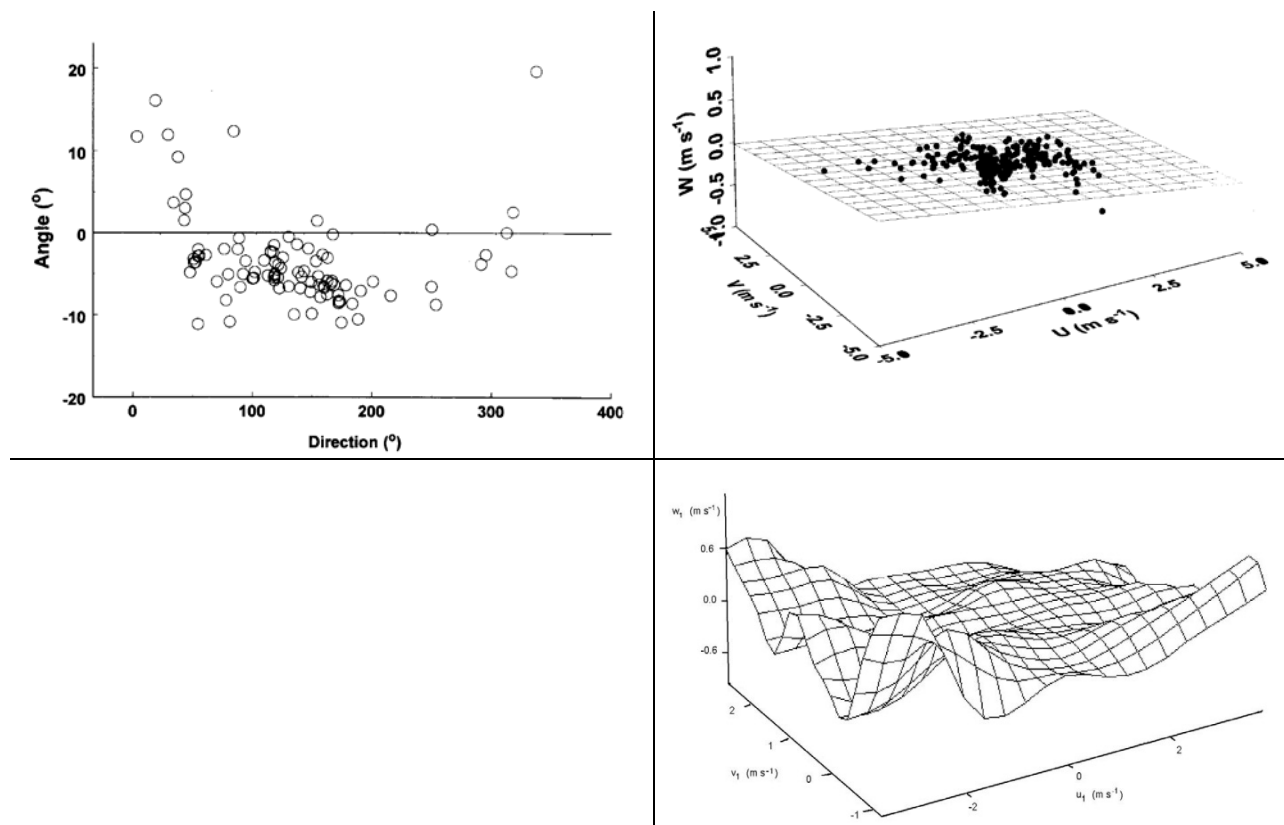
Figure 2. Tilt correction at the Wind River Canopy Crane Facility, WA, U.S.A. as a function of flow direction. Upper left panel: vertical transform angle as a function of horizontal wind direction (taken from Paw U et al., 2000); upper right panel: fitting of an aerodynamic plane (taken from Paw U et al., 2000); lower right panel: fitting of an aerodynamic surface (taken from Lee et al., 2004)

4.1.4   Summary of coordinate rotation methods

Table 3 provides an overview of the advantages and disadvantages of the three coordinate rotation methods. The main advantages of the double rotation method are its applicability for online flux computation, and its robustness against alignment changes of the SONIC. However, the method also suffers from several disadvantages which are overcome by the PF and surface fit methods. In particular, instrument offsets, low wind periods or transient mean vertical flows $\overline{w} \neq 0$ can result in over-rotation. E.g., 0.05 m s^{-1} mean vertical flow at 2 m s^{-1} mean horizontal flow results in 1.5° over-rotation. Errors >10% per 1° over-rotation and ≤5% per 2° over-rotation have been reported for measurements of shear stress (Wilczak et al., 2001) and scalar flux (Lee et al., 2004), respectively. These errors are not distributed randomly, but a function of the 3-D flow pattern at the measurement site. Over complex terrain with diurnal flow patterns, resulting biases of the daily flux integrals in the order of 5% have been observed (Turnipseed et al., 2003).

In contrast, the PF and surface fit methods eliminate over-rotation by identifying and distinguishing (i) an ensemble mean regression offset, and (ii) the transient mean vertical flows during each averaging period. For flows over uniformly tilted slopes the PF method is applicable, while over more complex surfaces only the surface fit method is capable of this differentiation. The transient mean vertical flows can contribute up to 25% to the total surface-atmosphere exchange over complex topography (Finnigan et al., 2003), and are only quantifiable with the latter regression methods. Moreover, these methods (i) avoid high-pass filtering and cross-axis folding, (ii) provide a consistent frame of reference to assess the quality of the EC-TES flux measurement over multiple days, (iii) enable tracking of the instrument alignment, and (iv) enable quantification of the uncertainty related to coordinate rotations.

Table 3. Properties of three coordinate rotation methods for the alignment of the EC-TES measurements with the mean streamlines. Advantages of individual methods are highlighted with underline.

Property	Double rotation	Planar fit	Surface fit
Vector basis	Average streamline	Aerodynamic plane	Aerodynamic surface
Data basis	Individual averaging period	Ensemble of averaging periods	Ensemble of averaging periods
Computation	Real-time	Delayed	Delayed
Change in anemometer alignment	Automatic adaptation	New set of rotation angles required	New set of rotation angles required
Over-rotation	Problematic	Eliminated for simple slopes	Eliminated for complex terrain
Information on vertical advection	No	For simple slopes	For complex terrain
High-pass filtering and cross-axis folding	Yes	No	No
Consistent vector basis for flux QA/QC	No	Yes	Yes
Tracking instrument tilt	No	Yes	Yes
Uncertainty propagation	No	Yes	Yes

4.2   Theory of algorithm

Goldstein et al. (2001), Wilczak et al. (2001) define a transform between the wind components $\bar{u}$, $\bar{v}$, $\bar{w}$ in the streamwise vector basis x, y, z, and the measured wind components $\overline{u_m}$, $\overline{v_m}$, $\overline{w_m}$ in the vector basis of an anemometer x_m, y_m, z_m;

$$\begin{bmatrix} \overline{u_m} \\ \overline{v_m} \\ \overline{w_m} \end{bmatrix} = \mathbf{T}(\alpha, \beta, \varPsi_{ms}) \begin{bmatrix} \bar{u} \\ \bar{v} \\ \bar{w} \end{bmatrix}. \tag{1}$$

The direction cosine matrix $\mathbf{T}(\alpha, \beta, \varPsi_{ms})$ between the two vector bases is specified by three Euler angles, α, β, and $\varPsi_{ms}$, which define three successive rotations about three orthogonal axes (Figure 3). The first rotation is the pitch α about the original y-axis; the second rotation is the roll β about the intermediate x-axis; and the third rotation is the yaw $\varPsi_{ms}$ about the final z-axis. In each step a positive rotation angle is defined as a clockwise rotation from the original to the transformed vector basis, when looking down the axis of rotation toward the origin. When using matrix multiplications the order of rotations is not commutative, and Wilczak et al. (2001) refer to this rotation order as the *y-x-z* convention. Each of the three individual rotations can be expressed in terms of the rotation matrices $\mathbf{A}(\alpha)$, $\mathbf{B}(\beta)$, and $\mathbf{C}(\varPsi_{ms})$;

$$\mathbf{A}(\alpha) = \begin{bmatrix} \cos\alpha & 0 & \sin\alpha \\ 0 & 1 & 0 \\ -\sin\alpha & 0 & \cos\alpha \end{bmatrix}, \tag{2}$$

$$\mathbf{B}(\beta) = \begin{bmatrix} 1 & 0 & 0 \\ 0 & \cos\beta & -\sin\beta \\ 0 & \sin\beta & \cos\beta \end{bmatrix}, \tag{3}$$

$$\mathbf{C}(\varPsi_{ms}) = \begin{bmatrix} \cos\varPsi_{ms} & -\sin\varPsi_{ms} & 0 \\ \sin\varPsi_{ms} & \cos\varPsi_{ms} & 0 \\ 0 & 0 & 0 \end{bmatrix}, \tag{4}$$

which yield the direction cosine matrix $\mathbf{T}(\alpha, \beta, \varPsi_{ms})$;

$$\mathbf{T}(\alpha, \beta, \varPsi_{ms}) = \mathbf{C}(\varPsi_{ms})\mathbf{B}(\beta)\mathbf{A}(\alpha). \tag{5}$$
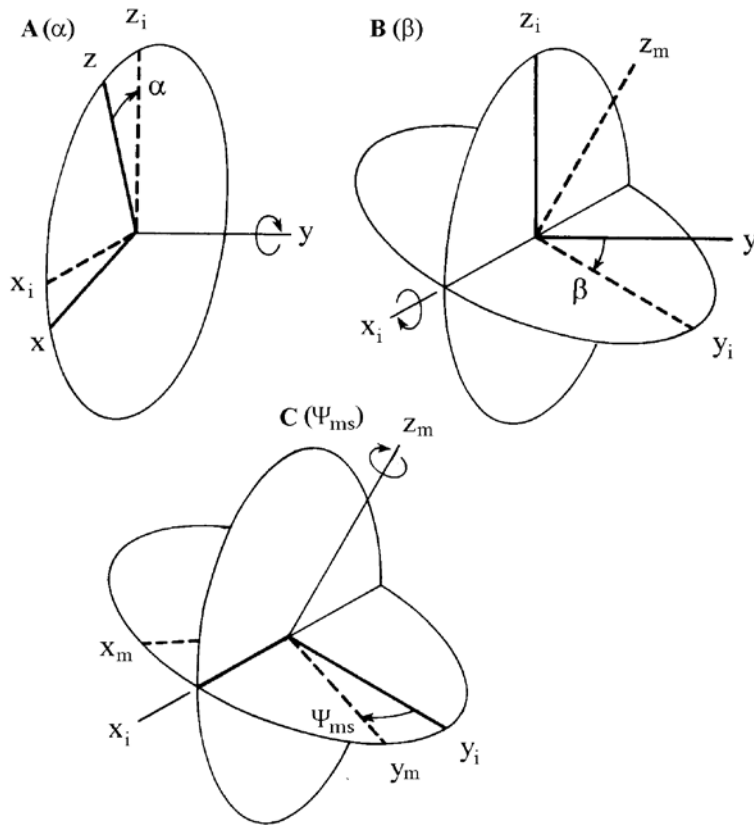
Figure 3. Modified after Wilczak et al. (2001): Definition of the rotations $\mathbf{A}(\alpha)$, $\mathbf{B}(\beta)$, and $\mathbf{C}(\Psi_{ms})$ for the *y-x-z* convention. The axes of the streamwise vector basis are *x*, *y*, *z*, the intermediate axes are x_i, y_i, and z_i, and the axes in the anemometer vector basis are x_m, y_m, z_m.

Because the matrices $\mathbf{A}(\alpha)$, $\mathbf{B}(\beta)$, and $\mathbf{C}(\Psi_{ms})$ are orthogonal, so is matrix $\mathbf{T}(\alpha, \beta, \Psi_{ms})$, and the inverse of $\mathbf{T}(\alpha, \beta, \Psi_{ms})$ is equal to its transpose, $\mathbf{T}^{-1}(\alpha, \beta, \Psi_{ms}) = \mathbf{T}^T (\alpha, \beta, \Psi_{ms})$. Hence, the procedure is reversible, and the anemometer vector basis can be transformed into a streamwise vector basis (Wilczak et al., 2001);

$$\begin{bmatrix} \overline{u} \\ \overline{v} \\ \overline{w} \end{bmatrix} = \mathbf{T}^T(\alpha, \beta, \Psi_{ms}) \begin{bmatrix} \overline{u_m} \\ \overline{v_m} \\ \overline{w_m} \end{bmatrix},$$

(6)

with the ordered rotations around the angles α, β, and Ψ_{ms};

(7)

$$\mathbf{T}^T = \mathbf{A}^T(\alpha)\, \mathbf{B}^T(\beta)\, \mathbf{C}^T(\Psi_{ms}).$$

4.3 Special considerations

In the following section the wind- and scalar flux vector, as well as the shear stress tensor are rotated into a streamwise vector basis. For relating the resulting variables to estimates of the true surface-air exchange, Finnigan (1999), Finnigan et al. (2003) add a word of caution which will be addressed during the implementation of AD[01];

(i) All the other terms contributing to the mass balance, such as the storage term must also be rotated into the same vector basis to represent the identical control volume;

(ii) By rotation of the vector basis, also the area of ground surface that is represented by the EC-TES measurement changes. This has to be taken into account by the cosine law;

(iii) When using the PF or surface fit rotation methods, the long term mean vertical wind $\hat{w}$ is forced to zero, while the mean vertical wind $\overline{w}$ during individual averaging periods can differ from zero. The identification of non-zero $\overline{w}$ avoids over-rotation as encountered during the double rotation procedure. Vertical advection through non-zero $\overline{w}$ results from (i) transient low-frequency contributions to the true surface-air exchange, which are neglected in the inner covariance for the duration of the averaging periods, and (ii) compensatory flows in response to horizontal divergence. While we are interested in the former, the latter can temporarily result in large magnitude and scatter in the measured vertical advection. Finnigan et al. (2003) present a procedure to isolate the net contribution of transient low-frequency motions to the true surface-air exchange. The procedure assumes that horizontal divergence tends to cancel out over longer timescales, such as a full diurnal cycle. Consequently the outer covariance of mean wind and scalar concentration between the averaging periods can be used as a quantitative indicator for unaccounted low-frequency flux contributions.

5 ALGORITHM IMPLEMENTATION

NEON uses the well-established PF method (Wilczak et al., 2001) to operationally provide high-quality observations of the turbulent part, and corresponding information on the non-turbulent part of the surface-atmosphere exchange. While overcoming fundamental shortcomings of the double rotation method, the PF method does not require similarly large data sets as the surface fit methodology does. This enables applying the PF method on a moving-average basis, which mediates operational concerns such as changes in anemometer alignment (e.g., Kaimal and Haugen, 1969 propose a 0.1° accuracy threshold) and near-real-time computation.

In the following, an averaging period refers to the length of non-overlapping, subsequent time windows which are used for the computation of the block averaged wind components $\overline{u_{\mathrm{m}}}$, $\overline{v_{\mathrm{m}}}$, $\overline{w_{\mathrm{m}}}$ (calculation of averages, variances and covariances is defined in AD[04]). For turbulence measurements often a 0.5 h period is used for the averaging period, each resulting in an independent observation of $\overline{u_{\mathrm{m}}}$, $\overline{v_{\mathrm{m}}}$, $\overline{w_{\mathrm{m}}}$. The PF method utilizes ensembles of these observations to obtain a suitable sample size. We refer to the

corresponding time interval as the PF period, which typically ranges from days to months (e.g., Mauder et al., 2006, Yuan et al., 2011).

5.1 Determination of rotation angles

The PF method determines a single pair of pitch rotation angle $\hat{\alpha}$ and roll rotation angle $\hat{\beta}$ for the entire PF period (indicated by the caret/circumflex/hat symbol). In contrast, the azimuth rotation angle $\overline{\varPsi_{ms}}$ (i.e., the wind direction) is determined individually for each averaging period (indicated by the overbar). The tilted plane that minimizes the ensemble mean vertical wind over the PF period can be expressed by the coefficients of a multiple linear regression (Wilczak et al., 2001);

$$\overline{w_m} = \widehat{w_0} + \widehat{c_{ms,1}}\ \overline{u_m} + \widehat{c_{ms,2}}\ \overline{v_m}. \tag{8}$$

Once the constant regression offset $\widehat{w_0}$, the regression slopes $\widehat{c_{ms,1}}$, $\widehat{c_{ms,2}}$ and their uncertainties $\sigma(\widehat{w_0})$, $\sigma(\widehat{c_{ms,1}})$, and $\sigma(\widehat{c_{ms,2}})$ are known, the rotation angles $\hat{\alpha}$, $\hat{\beta}$ can be determined as (Wilczak et al., 2001);

$$\hat{\alpha} = \sin^{-1}(\widehat{c_{31}}), \tag{9}$$

$$\hat{\beta} = \sin^{-1}\left(\frac{-\widehat{c_{32}}}{\sqrt{\widehat{c_{32}}^2 + \widehat{c_{33}}^2}}\right), \text{ with} \tag{10}$$

$$\widehat{c_{31}} = \frac{-\widehat{c_{ms,1}}}{\sqrt{\widehat{c_{ms,1}}^2 + \widehat{c_{ms,2}}^2 + 1}}, \tag{11}$$

$$\widehat{c_{32}} = \frac{-\widehat{c_{ms,2}}}{\sqrt{\widehat{c_{ms,1}}^2 + \widehat{c_{ms,2}}^2 + 1}}, \tag{12}$$

$$\widehat{c_{33}} = \frac{1}{\sqrt{\widehat{c_{ms,1}}^2 + \widehat{c_{ms,2}}^2 + 1}}. \tag{13}$$

5.2 Rotation into the planar fit vector basis

The pitch and roll rotation angles $\hat{\alpha}$, $\hat{\beta}$ apply to the entire PF period. In contrast, the azimuth rotation angle $\overline{\varPsi_{ms}}$ has to be calculated for each averaging period individually;

$$\overline{\varPsi_{ms}} = \tan^{-1}\left(\frac{\overline{v_{ms}}}{\overline{u_{ms}}}\right), \tag{14}$$

using the wind components in the plane of the mean streamlines (subscript ms, Wilczak et al., 2001);

$$
\begin{bmatrix} \overline{u_{\mathrm{ms}}} \\ \overline{v_{\mathrm{ms}}} \\ \overline{w_{\mathrm{ms}}} \end{bmatrix} = \mathbf{A}^{\mathrm{T}}(\hat{\alpha}) \, \mathbf{B}^{\mathrm{T}}(\hat{\beta}) \begin{bmatrix} \overline{u_{\mathrm{m}}} \\ \overline{v_{\mathrm{m}}} \\ \overline{w_{\mathrm{m}}} \end{bmatrix}.
\tag{15}
$$

After all rotation angles $\hat{\alpha}$, $\hat{\beta}$, $\overline{\varPsi_{\mathrm{ms}}}$ are known, for each averaging period the measured vector and tensor quantities are rotated into the streamwise vector basis. The measured mean wind vector ($\overline{u_{\mathrm{m}}}$, $\overline{v_{\mathrm{m}}}$, $\overline{w_{\mathrm{m}}}$) is transformed using Eq. (6). In the context of this ATBD, no rotation is applied to the wind component raw data (20 Hz) measured by the SONIC. Instead, the relevant rotation angles $\hat{\alpha}$, $\hat{\beta}$, $\overline{\varPsi_{\mathrm{ms}}}$ are stored, which enables rotation of the raw data during implementation of AD[01]. The scalar covariance matrix is transformed using (Rebmann et al., 2012);

$$
\begin{bmatrix} \overline{u'X'} \\ \overline{v'X'} \\ \overline{w'X'} \end{bmatrix} = \mathbf{T}^{\mathrm{T}}(\hat{\alpha}, \hat{\beta}, \overline{\varPsi_{\mathrm{ms}}}) \begin{bmatrix} \overline{u'_{\mathrm{m}}X'} \\ \overline{v'_{\mathrm{m}}X'} \\ \overline{w'_{\mathrm{m}}X'} \end{bmatrix},
\tag{16}
$$

and the shear stress tensor is transformed using;

$$
\begin{bmatrix} \overline{u'u'} & \overline{u'v'} & \overline{u'w'} \\ \overline{v'u'} & \overline{v'v'} & \overline{v'w'} \\ \overline{w'u'} & \overline{w'v'} & \overline{w'w'} \end{bmatrix} = \mathbf{T}^{\mathrm{T}}(\hat{\alpha}, \hat{\beta}, \overline{\varPsi_{\mathrm{ms}}}) \begin{bmatrix} \overline{u'_{\mathrm{m}}u'_{\mathrm{m}}} & \overline{u'_{\mathrm{m}}v'_{\mathrm{m}}} & \overline{u'_{\mathrm{m}}w'_{\mathrm{m}}} \\ \overline{v'_{\mathrm{m}}u'_{\mathrm{m}}} & \overline{v'_{\mathrm{m}}v'_{\mathrm{m}}} & \overline{v'_{\mathrm{m}}w'_{\mathrm{m}}} \\ \overline{w'_{\mathrm{m}}u'_{\mathrm{m}}} & \overline{w'_{\mathrm{m}}v'_{\mathrm{m}}} & \overline{w'_{\mathrm{m}}w'_{\mathrm{m}}} \end{bmatrix} \mathbf{T}(\hat{\alpha}, \hat{\beta}, \overline{\varPsi_{\mathrm{ms}}}).
\tag{17}
$$

The resulting mean wind components and variances and covariances are orthogonal to the mean streamlines over the PF period.

5.3 Operational implementation

Table 4 provides a detailed processing order which specifies the operational implementation of the PF procedure. In short;

(i) Eq. (8) is solved using least-squares regression. No weighting procedure, e.g. with the inverse variance in the wind components is used. Such procedure would favor night-time measurements with low wind variances over day-time measurements with high wind variances.

(ii) The length of an averaging period is 0.5 h, the default length of a PF period is t_{PF}=168 h. The PF coefficients are recalculated every 24 h, i.e. the PF window moves with a 'step size' of 24 h through the data, and the derived PF coefficients are applicable for the 24 h in the center of t_{PF}. The default length of t_{PF} is chosen to enable reflecting changes in the environmental forcing that affect the mean streamline, such as the passage of weather systems or ecosystem phenology. On the other hand, the length of t_{PF} shall also be long enough to approach zero average vertical wind, and to warrant a sample size that is sufficient for the reliable fitting of an aerodynamical plane. If the length of t_{PF} will proof unfeasible at individual sites, a site-specific (shorter or longer) PF period will be assigned. The duration of t_{PF} for each

site shall be stored in the Cyberinfrastructure data store. Hence, a default PF period contains N_{PF} = 168 h x 2 averaging periods = 336 averaging periods, which is the basic sample size used in the regression step (i). This sample size is further reduced as detailed in the following.

(iii) A flagging procedure is used to exclude unsuitable averaging periods from the determination of the rotation angles (Sect. 5.1). By default, the quality flags for all averaging periods are set to 0.

- A quality flag $QF_{pitch,2,i}$ is set to 1 for an averaging period (subscript i) if the variability in SONIC pitch exceeds a threshold of 0.1°. This threshold is required to determine turbulent fluxes to within 1% tilt error (Sect. 4.1.4);
- A quality flag $QF_{roll,2,i}$ is set to 1 for an averaging period if the variability in SONIC roll exceeds a threshold of 0.1°;
- A quality flag $QF_{magn,i}$ is set to 1 for an averaging period if the magnitude of the wind vector is outside the 10–90% percentile for the given PF period (least-squares regression is sensitive to outliers;
- A quality flag $QF_{PF,i}$ is set to 1 for an averaging period if (i) one or more of the above conditions apply, or (ii) $QM_{hard,i}$ > 10% for one or more of $\overline{u_m}$, $\overline{v_m}$, $\overline{w_m}$. $QM_{hard,i}$ is derived in AD[04], and expresses the percentage of high-frequency observations that was discarded in each averaging period due to one or more of the following conditions; (i) the SONIC is being heated; (ii) instrument flags indicate malfunction; (iii) statistical QA/QC flags indicate unfeasible measurement values; (iv) magnitude of SONIC pitch and/or roll exceed required thresholds; (v) boom arm accelerations exceed required thresholds; (vi) the boom arm is being maintained; (vii) the horizontal inflow sector is potentially subject to flow distortion from the tower infrastructure;
- Only averaging periods for which $QF_{PF,i}$ = 1 are used for the determination of the rotation angles;
- The quality flag $QF_{window,i}$ is used to record whether a trailing ($QF_{window,i}$ = −7), centered ($QF_{window,i}$ = 3) or leading ($QF_{window,i}$ = 7) PF period is used for the determination of the rotation angles. Also, $QF_{window,i}$ = −3 indicates when the rotation angles of the preceding PF period are used due to a lack of suitable data in the present PF period.

(iv) Lastly, the actual rotation per Eqs. (6), (16)–(17) are performed.

An additional condition to reject averaging periods under diabatic stratification was proposed by Finnigan (1999). No such condition is applied here, in an attempt to optimize the tradeoff between sufficiently large sample size and relatively short PF periods.

Table 4. Processing order for the implementation of the PF regression and the rotation into the streamwise base vector.

Parameter	Processing order
Averaging period	Every 0.5 h, starting on the full/half hour and continuing up to but not including the next full/half hour, and coordinated across all product instances.
Applicable period for $\hat{\alpha}$, $\hat{\beta}$, $\widehat{w_0}$ ($t_{\alpha,\beta,w0}$)	24 h, starting 00:00:00.00 and continuing up to but not including 24:00:00.00 local standard time (no daylight saving adjustment).
Applicable period for $\overline{\Psi_{ms}}$ ($t_{\Psi,ms}$)	Every 0.5 h, starting on the full/half hour and continuing up to but not including the next full/half hour, and coordinated across all product instances.
PF period (t_{PF})	168 h centered time window, extending 72 h before and 72 h after $t_{\alpha,\beta,w0}$.
Quality flags	Assign value of 0 to all of $QF_{magn,i}$, $QF_{PF,i}$, $QF_{pitch,2,i}$, $QF_{roll,2,i}$, $QF_{window,i}$ for all averaging periods in t_{PF}. Flag averaging periods for which $QM_{hard,i}(u_m) > 10\%$ | $QM_{hard,i}(v_m) > 10\%$ | $QM_{hard,i}(w_m) > 10\%$. Assign $QF_{PF,i} = 1$ to corresponding averaging periods in t_{PF}.
SONIC pitch and roll	Flag averaging periods with excessive SONIC pitch variations over t_{PF}, i.e., $\left|\overline{\theta_1} - \hat{\theta}\right| > 0.1°$. Assign $QF_{PF,i} = 1$ and $QF_{pitch,2,i} = 1$ to corresponding averaging periods in t_{PF}. Flag averaging periods with excessive SONIC roll variations over t_{PF}, i.e., $\left|\overline{\phi_1} - \hat{\phi}\right| > 0.1°$. Assign $QF_{PF,i} = 1$ and $QF_{roll,2,i} = 1$ to corresponding averaging periods in t_{PF}.
Wind vector magnitude	Flag averaging periods outside the 10%–90% percentile of $\sqrt{\overline{u_m}^2 + \overline{v_m}^2 + \overline{w_m}^2}$ over t_{PF}. Assign $QF_{PF,i} = 1$ and $QF_{magn,i} = 1$ to corresponding averaging periods in t_{PF}.
Update of $\hat{\alpha}$, $\hat{\beta}$, $\widehat{w_0}$	Every subsequent $t_{\alpha,\beta,w0}$ (every 24 h); (i) If N ($QF_{PF,i} = 0$) ≥ 200 averaging periods are available within t_{PF}, perform update and assign $QF_{window,i} = 3$ to all averaging periods in $t_{\alpha,\beta,w0}$ (Yuan et al., 2011). (ii) If N ($QF_{PF,i} = 0$) < 200, do not perform update, but re-use the parameter set $\hat{\alpha}$, $\hat{\beta}$, $\widehat{w_0}$ of the preceding $t_{\alpha,\beta,w0}$. Assign $QF_{window,i} = -3$ to all averaging periods in the current $t_{\alpha,\beta,w0}$.
Boom arm maintenance	When field maintenance is performed on the boom arm ($QF_{boom,i} = 1$), the update cycle of $\hat{\alpha}$, $\hat{\beta}$, $\widehat{w_0}$ is interrupted.

Parameter	Processing order
	(i) The parameter set $\hat{\alpha}$, $\hat{\beta}$, $\widehat{w_0}$ is evaluated for a 168 h trailing time window, extending 168 h before (including) the last full $t_{\psi,ms}$ preceding field maintenance. The resulting parameter set $\hat{\alpha}$, $\hat{\beta}$, $\widehat{w_0}$ is used for all averaging periods after (excluding) the last full $t_{\alpha,\beta,w0}$, until (including) the last full $t_{\psi,ms}$ preceding field maintenance. Assign $QF_{window,i} = -7$ to all averaging periods in this time window. (ii) The parameter set $\hat{\alpha}$, $\hat{\beta}$, $\widehat{w_0}$ is evaluated for a 168 h leading time window, extending 168 h after (including) the first full $t_{\psi,ms}$ after field maintenance. The resulting parameter set $\hat{\alpha}$, $\hat{\beta}$, $\widehat{w_0}$ is used for all averaging periods after (including) the first full $t_{\psi,ms}$ after field maintenance, until (excluding) the first full $t_{\alpha,\beta,w0}$. Assign $QF_{window,i} = 7$ to all averaging periods in this time window.
Update of $\overline{\Psi_{ms}}$	Every subsequent $t_{\psi,ms}$ (every 0.5 h).
Perform rotation	Perform Eqs. (6), (16)–(17) individually for each averaging period in $t_{\alpha,\beta,w0}$, with values for $\hat{\alpha}$, $\hat{\beta}$, $\overline{\Psi_{ms}}$ as specified above.

The following variables shall be reported as results of this ATBD, i.e. they shall be made available as input variables for subsequent ATBDs. During the implementation of AD[01], these ABTDs will be combined and corresponding DPs will be defined;

(i) Individually for each averaging period in t_{PF};

- Quality flags QF_{magn}, QF_{PF}, $QF_{pitch,2}$, $QF_{roll,2}$.

(ii) Individually for each averaging period in $t_{\alpha,\beta,w0}$;

- azimuth angle ($\overline{\Psi_{ms}}$);
- rotated averages ($\bar{u}$, $\bar{v}$, $\bar{w}$);
- rotated variances ($\overline{u'u'}$, $\overline{v'v'}$, $\overline{w'w'}$);
- rotated covariances ($\overline{u'X'}$, $\overline{v'X'}$, $\overline{w'X'}$).

(iii) Identical for all averaging periods in $t_{\alpha,\beta,w0}$;

- Quality flag QF_{window};
- PF results ($\widehat{w_0}$, $\hat{\alpha}$, $\hat{\beta}$);
- Sample sizes N_{PF}, $N(QF_{magn} = 0)$, $N(QF_{PF} = 0)$, $N(QF_{pitch,2} = 0)$, $N(QF_{roll,2} = 0)$.

6 UNCERTAINTY

This section concerns only the propagation of sensor/calibration uncertainty in the input variables, through the presented algorithms, into the variables reported in this ATBD. This section does not concern testing the fulfillment of assumptions in the EC method, quantification of sampling errors and the like. These sources of uncertainty are addressed in a series of tests during the implementation of AD[01] (details provided therein).

Once all higher-level NEON data products are mapped out, an integrated uncertainty propagation plan will be derived. At the present time this section represents a simplified indicator for the potential direction of such uncertainty propagation plan. For this purpose resolution is defined as the smallest detectable change in a variable, and accuracy and precision as the systematic and random uncertainties in a variable, respectively. In the following generic algorithms are provided that enable the propagation of resolution, accuracy and precision through Eqs. (1)–(17).

6.1 Analysis of uncertainty

Following Taylor (1997) the maximum probable error σ_A of a function F with *N* input variables (*X*) is defined as;

$$\sigma_A(F) = \sum_{i=1}^{N} \left| \frac{\partial F}{\partial X_i} \right| \sigma_A(X_i). \tag{18}$$

The partial derivative $\partial F/\partial X_i$ is the slope of F with X_i, and hence quantifies the sensitivity of F on uncertainty in X_i. In the following Eq. (18)(18) is used as model for the propagation of accuracy (subscript A) through Eqs. (1)–(17). If random and independent, the uncertainties in X_i tend to cancel, and Gaussian quadrature applies;

$$\sigma_P^2(F) = \sum_{i=1}^{N} \left(\frac{\partial F}{\partial X_i} \sigma_P(X_i) \right)^2. \tag{19}$$

Eq. (19)(19) is used as model for the propagation of precision (subscript P) and resolution through Eqs. (1)–(17). At this point it is assumed that the resolution follows a binomial distribution (low amplitude noise between two adjacent discrete values, Vickers and Mahrt, 1997). For sufficiently large sample sizes (20 or greater, Box et al., 2005), the binomial distribution is reasonably approximated by the normal distribution, and can be quantified by Gaussian metrics such as Eq. (19)(19).

6.2 Reported uncertainty

In order to calculate the accuracy, precision and resolution for each reported variable in Table 1, the partial derivatives of Eqs. (1)–(17) shall be found, and combined in accordance with Eqs. (18)–(19).

Eq. (19) analogously applies for the determination of the resulting resolution, when replacing the precisions (standard deviations) σ_P with the resolutions (finite differences) Δ_R.

7 ALGORITHM VERIFICATION

Verification of the algorithms disclosed in this ATBD shall follow the procedures outlined in AD[05]. During the implementation of AD[01], DPs will be derived from the present algorithms, and DP verification and validation will be specified accordingly.

8 SCIENTIFIC AND EDUCATIONAL APPLICATIONS

Placing surface-air exchange measurements into a streamwise frame of spatial reference is the basis for processing turbulence data into higher-level DPs with ecological relevance. The present ATBD details all relevant transformations and uncertainty propagation related to rotating the turbulent exchange measurements by the EC-TES into the PF base vector. During the implementation of AD[01], data will continue to be processed into higher-level DPs. Ecologically relevant high-level DPs from the EC-TES include the exchange of heat, water vapor and CO_2 between the land surface and the atmosphere. These DPs are used for constraining, calibrating and validating process-based models (e.g., Rastetter et al., 2010). This shall enable the detection of continental scale ecological change and the forecasting of its impacts.

Standardized and transparent documentation intends to foster reproducibility of all data processing steps. For this purpose, it is planned to make all processing steps available as open-source code in a high-level programming language. Aside from enabling direct feedback from the research community, this also provides community members (e.g. students at graduate level) a straightforward and hands-on toolbox for data processing of micrometeorological measurements.

9 FUTURE PLANS AND MODIFICATIONS

This ATBD will be version controlled, i.e. future developments might results in modifications to this ATBD, which will be documented accordingly.

For example, this ATBD discusses several methods for aligning a Cartesian coordinate system with the local streamlines. The PF method is chosen for this purpose, as it overcomes fundamental shortcomings of the double rotation method, and does not require similarly large data sets as the surface fit methodology does. However, this choice may change in the future following scientific developments, and would be documented in a revision of this ATBD For example, the PF method has been successfully applied also over complex topography (e.g., Turnipseed et al., 2003). However, the surface fit method might more appropriately reproduce the actual field of streamlines in such settings, and better fulfill the assumption of measuring the surface-air exchange perpendicular to the terrain surface.

10 APPENDIX

10.1 Acronyms

Acronym	Description
1-D	One-dimensional
3-D	Three-dimensional
ATBD	Algorithm theoretical basis document
C^3	Command, control, and configuration document
CO_2	Carbon dioxide
DP	Data product
EC	Eddy covariance
EC-TES	Eddy-covariance turbulent exchange subsystem
FIU	Fundamental instrument unit (NEON project team)
NEON	National Ecological Observatory Network
PF	Planar fit
QA/QC	Quality Assurance/Quality Control
SONIC	Ultrasonic anemometer/thermometer

10.2 Functions

Function	Description
|	Logical operator – OR
A, **B**, **C**, **T**	Direction cosine matrices
∂	Partial differential operator
Δ	Finite difference operator
F	Function for error propagation
σ	Standard deviation

Function	Description
$\bar{X}$	Short-term (e.g., 30 min) arithmetic mean of atmospheric quantity X
$\hat{X}$	Longer-term (e.g., 1 week) arithmetic mean of atmospheric quantity X
$\overline{X'X'}, \overline{X'^2}$	Short-term (e.g., 30 min) sample variance of atmospheric quantity X
$\overline{X'Y'}$	Short-term (e.g., 30 min) sample covariance of atmospheric quantities X and Y

10.3 Parameters

Parameter	Description	Numeric value	Units
c	Constant, coefficient	User-defined	User-defined
N	Sample size	User-defined	Dimensionless (count)

10.4 Subscripts

Subscript	Description
1…N	Numeric identifier
A	Accuracy
hard	Measurement or instrument conditions that do not permit data usage
i	Running index
m	Measurement
ms	In the plane of the mean streamlines
P	Precision
PF	Planar fit
R	Resolution
soft	Measurement or instrument conditions that are potentially suspicious
x, y, z	Along-, cross- and vertical axes of a Cartesian coordinate system

10.5 Variables

Variable	Description	Units
α, β	Planar fit pitch and roll rotation angles	Decimal degree
d	distance/length/height	m
$d_{x,FP90}$	Cross-wind integrated upwind extent from within which 90% of an observed value is sourced	m
$d_{z,d}$	displacement height	m
θ	Sonic anemometer pitch	Decimal degree
i	Running index	Dimensionless (count)
QF	Quality flag	Dimensionless (0 or 1)
QF_{magn}, QF_{PF}, $QF_{pitch,2}$, $QF_{roll,2}$, QF_{window}	Coordinate rotation quality flags	Dimensionless (0 or 1)
QF_{boom}	Flag for turbulence boom maintenance	Dimensionless (0 or 1)
QM	Quality metric	%
$t_{\alpha,\beta,w0}$	Applicable period for the planar fit results of pitch rotation angle (α), roll rotation angle (β), and regression offset (w_0)	Hours (h)
t_{PF}	Duration of a planar fit period	Hours (h)
$t_{\Psi,ms}$	Applicable period for the planar fit result of azimuth rotation angle/wind direction (Ψ_{ms})	Hours (h)
u, v, w	Along-, cross- and vertical wind speed	m s^{-1}
V	Control volume	m^3
w_0	Vertical wind offset	m s^{-1}
ϕ	Sonic anemometer roll	Decimal degree

Variable	Description	Units
x, y, z	Along-, cross- and vertical axes of a Cartesian coordinate system	Dimensionless
X	Placeholder for atmospheric quantity	Depending on unit of atmospheric quantity
Ψ	Wind direction	Decimal degree

11 BIBLIOGRAPHY

Aubinet, M., Feigenwinter, C., Heinesch, B., Laffineur, Q., Papale, D., Reichstein, M., Rinne, J. & Van Gorsel, E. (2012) Nighttime flux correction. *Eddy covariance: A practical guide to measurement and data analysis* (eds M. Aubinet, T. Vesala & D. Papale), pp. 211-261. Springer, Dordrecht, Heidelberg, London, New York.

Baldocchi, D., Finnigan, J., Wilson, K., Paw U, K. T. & Falge, E. (2000) On Measuring Net Ecosystem Carbon Exchange Over Tall Vegetation on Complex Terrain. *Boundary-Layer Meteorology,* 96, 257-291.

Box, G. E. P., Hunter, J. S. & Hunter, W. G. (2005) *Statistics for experimenters: design, innovation, and discovery.* John Wiley & Sons, New York, Chichester, Brisbane, Toronto, Singapore.

Finnigan, J. (1999) A comment on the paper by Lee (1998): "On micrometeorological observations of surface-air exchange over tall vegetation". *Agricultural and Forest Meteorology,* 97, 55-64.

Finnigan, J. J. (2004) A re-evaluation of long-term flux measurement techniques. Part 2: Coordinate systems. *Boundary-Layer Meteorology,* 113, 1-41.

Finnigan, J. J., Clement, R., Malhi, Y., Leuning, R. & Cleugh, H. A. (2003) A re-evaluation of long-term flux measurement techniques. Part 1: Averaging and coordinate rotation. *Boundary-Layer Meteorology,* 107, 1-48.

Foken, T. (2008) *Micrometeorology.* Springer, Berlin, Heidelberg.

Goldstein, H., Poole, C. & Safko, J. (2001) *Classical Mechanics (3rd Edition).* Addison Wesley, Boston, Massachusetts.

Kaimal, J. C. & Finnigan, J. J. (1994) *Atmospheric boundary layer flows: Their structure and measurement.* Oxford University Press, New York.

Kaimal, J. C. & Haugen, D. A. (1969) Some Errors in the Measurement of Reynolds Stress. *Journal of Applied Meteorology,* 8, 460-462.

Kondo, J. & Sate, T. (1982) The Determination of the von Kármán Constant. *Journal of the Meteorological Society of Japan,* 60, 461-471.

Lee, X. (1998) On micrometeorological observations of surface-air exchange over tall vegetation. *Agricultural and Forest Meteorology,* 91, 39-49.

Lee, X., Finnigan, J. & Paw U, K. T. (2004) Coordinate systems and flux bias error. *Handbook of micrometeorology: A guide for surface flux measurement and analysis* (eds X. Lee, B. Law & W. Massman), pp. 33-66. Springer, Dordrecht.

Mahrt, L., Vickers, D., Howell, J., Højstrup, J., Wilczak, J. M., Edson, J. & Hare, J. (1996) Sea surface drag coefficients in the Risø Air Sea Experiment. *Journal of Geophysical Research,* 101, 14327-14335.

Mauder, M., Liebethal, C., Göckede, M., Leps, J. P., Beyrich, F. & Foken, T. (2006) Processing and quality control of flux data during LITFASS-2003. *Boundary-Layer Meteorology,* 121, 67-88.

McMillen, R. T. (1988) An eddy correlation technique with extended applicability to non-simple terrain. *Boundary-Layer Meteorology,* 43, 231-245.

Paw U, K. T., Baldocchi, D. D., Meyers, T. P. & Wilson, K. B. (2000) Correction Of Eddy-Covariance Measurements Incorporating Both Advective Effects And Density Fluxes. *Boundary-Layer Meteorology,* 97, 487-511.

Rannik, Ü. (1998) On the surface layer similarity at a complex forest site. *Journal of Geophysical Research,* 103, 8685-8697.

Rastetter, E. B., Williams, M., Griffin, K. L., Kwiatkowski, B. L., Tomasky, G., Potosnak, M. J., Stoy, P. C., Shaver, G. R., Stieglitz, M., Hobbie, J. E. & Kling, G. W. (2010) Processing arctic eddy-flux data using a simple carbon-exchange model embedded in the ensemble Kalman filter. *Ecological Applications,* 20, 1285-1301.

Rebmann, C., Kolle, O., Heinesch, B., Queck, R., Ibrom, A. & Aubinet, M. (2012) Data acquisition and flux calculations. *Eddy covariance: A practical guide to measurement and data analysis* (eds M. Aubinet, T. Vesala & D. Papale), pp. 59-83. Springer, Dordrecht, Heidelberg, London, New York.

Schmid, H. P. (1994) Source areas for scalars and scalar fluxes. *Boundary-Layer Meteorology,* 67, 293-318.

Tanner, C. B. & Thurtell, G. W. (1969) Anemoclinometer Measurements of Reynolds Stress and Heat Transport in the Atmospheric Surface Layer. pp. 200. University of Wisconsin, Madison.

Taylor, J. R. (1997) *An Introduction to Error Analysis: The Study of Uncertainties in Physical Measurements.* University Science Books, Mill Valley, California.

Turnipseed, A. A., Anderson, D. E., Blanken, P. D., Baugh, W. M. & Monson, R. K. (2003) Airflows and turbulent flux measurements in mountainous terrain: Part 1. Canopy and local effects. *Agricultural and Forest Meteorology,* 119, 1-21.

Vesala, T., Kljun, N., Rannik, U., Rinne, J., Sogachev, A., Markkanen, T., Sabelfeld, K., Foken, T. & Leclerc, M. Y. (2008) Flux and concentration footprint modelling: State of the art. *Environmental Pollution,* 152, 653-666.

Vickers, D. & Mahrt, L. (1997) Quality control and flux sampling problems for tower and aircraft data. *Journal of Atmospheric and Oceanic Technology,* 14, 512-526.

Wilczak, J. M., Oncley, S. P. & Stage, S. A. (2001) Sonic anemometer tilt correction algorithms. *Boundary-Layer Meteorology,* 99, 127-150.

Yuan, R., Kang, M., Park, S.-B., Hong, J., Lee, D. & Kim, J. (2011) Expansion of the planar-fit method to estimate flux over complex terrain. *Meteorology and Atmospheric Physics,* 110, 123-133.

12 CHANGELOG

Revision A, S. Metzger, et al. Initial Release.